POST ANNEALING EFFECT ON STRUCTURAL AND OPTICAL PROPERTIES OF (α-Fe_2O_3) THIN FILMS PREPARED BY SPRAY PYROLYSIS WITH MOVING NOZZLE

Y. MEFTAH[a,b], D. BEKKER[b], B. BENHAOUA[a,d*], A. RAHAL[a,b,d], A. BENHAOUA[a,b,d], A. H. HAMZAOUI[c]
[a]*Lab. VTRS, Faculty of Technology, Univ. El-Oued, El oued 39000, Algeria*
[b]*Faculty of Exact Sciences, Univ. El-Oued, El oued 39000, Algeria*
[c]*Centre National de Recherche en Sciences des Materiaux Tunisie*
[d]*Unité de Developpement des Energies Renouvelabes dans les Zones Arides, El oued 39000, Algeria*

Hematite iron oxide (α-Fe_2O_3) thin films were prepared using spray pyrolysis with moving nozzle. Effects of 0-3 hours post heat treatment at 550°C on their structural and optical properties have been studied. XRD analyses avowed the formation of hematite thin films structure along (*104*) and (*110*) as preferred orientations and intensities of which change with post annealing whereas the grain size was varied in 40-48 nm upon time heat treatment. SEM images showed that all sample having uniform morphology with variant shape upon post annealing time. The transparency of hematite thin films was averaged around 65% in the visible region, with an direct band gap in the range 2.11-2.13eV. FTIR study affirms the abundance of Fe-O bond in all samples. Results indicate that the best time of post-annealing was 2 hours.

(Received February 5, 2018; Accepted May 7, 2018)

Keywords : Thin film, Hematite Fe_2O_3, Spray pyrolysis, Post annealing, X-ray diffraction

1. Introduction

Iron oxides and hydroxides are among the most well-known metal oxides. The later is rich in nature, with sixteen known iron oxides and oxyhydroxides which may be readily synthesized in the laboratory. Of course, the iron oxides and oxyhydroxides in nature, their class of compounds have a rich palette of possible oxygen to iron ratios, as well as many different phases for each composition [1]. Iron compounds are of interest in a variety of scientific use, such asin catalysts [2], soil treatment [3-5], and in medical fields for anti-bacterial applications [6-8]. The stability and non-toxic nature of the iron oxides make them suitable for use as coatings [9, 10] and pigments. Previous studies showed that iron oxide covered sand has high competence for removing a range of contaminents from water/wastwater [11-13]. As pigments iron oxides have colors from yellow to brown and black;such change in colors was sugg ested to the electronic structure change with composition [14]. The three most common iron oxides forms in nature, which are technologically very important, are magnetite (Fe_3O_4), maghemite (γ-Fe_2O_3), and hematite (α-Fe_2O_3) respectively. Recently nanoparticles (NPs) of iron oxides are gaining more attention in environmental remediation due to their small sizes, large surface area and magnetic properties [15, 16]. Several methods are used in synthesizing iron oxide nanomaterials, which can be generally classified as physical, chemical and biological methods. Physical methods are still suffered from the inability to control the size of particles in the nanometer range [17]. The Fe_2O_3 thin film can be deposited by several techniques such as pulsed laser evaporation [18], physical vapor deposition [19] and so on.Chemical methods are samples,tractable, and efficient, in which the size, composition, and even the shape of the NPs can be managed [20], iron oxides can be synthesized through the co-precipitation of Fe^{2+} and Fe^{3+} by the addition of a base. The size, shape,

* Corresponding author : you.phy1988@gmail.com

and composition of iron oxides NPs synthesized through chemical methods depend on the type of used salt for instance chlorides [21], sulfates [22], and nitrates [23]. Also synthesized iron oxides NPs depends on ion Fe^{2+} and Fe^{3+} ratio, pH, and ionic strength [17]. Fe_2O_3 thin films can be deposited by Sol-gel [24], Electrodeposition method [25], Sonochemical [26], Electrospinning [27] and Spray pyrolysis method [28-31]. Chemical-based synthesis methods are mostly adopted due to low production cost and high yield.Finely biological methods have good reproducibility and scalability, high yield, and low cost [32, 33].

As reported above physical methods are still suffering from the inability to control the size of particles in the nanometer range; for instance, classical spray needs a stay in time to recuperate the substrate temperature (*i.e* losing more than 1hour to elaborate one sample). In an attempt to avoid this loss time, spray with amoving nozzle (SPMN) is used to uphold the heat of substrate during the elaborating period. The aim of this work is to synthesize and study physical properties of as (α-Fe_2O_3) and post annealing thin films with in the time, at 550°C using (SPMN) method.

2. Experimental details

2.1 Thin films preparation

Hematite α-Fe_2O_3 thin films were deposited on 500°C heated glass substrates (Ref:CAT.NO.7102, having 7.6x2.5x0.12cm^3 as dimensions) using a chemical spray pyrolysis technique with moving nozzle (SPMN).Moving nozzle and high deposition temperature are used to maintain the heat of substrate constant, and to eschew chlorine rubbles and to ensure thermal stability of the oxide respectively. The initial solution was prepared by dissolving iron chloride $FeCl_3$ at a concentration of 0.5M in double distilled water and methanol in a volume ratio (1:1), the solution was stirred, for 60min, using a magnetic stirrer to release complete dissolution. The obtained solution was sprayed on cleaned glass via the moving nozzle at constant velocity (10cm/min); The deposition time was 3min with spray rate of 5ml/min with kept distance nozzle-substrate of about 5cm. Usually, the formed thin films were orange brownish in color as shown in Fig.1. For post-annealing treatment at 550°C for different dwelling times (0,1, 2, and 3 hours), the deposited thin films were placed in a high-temperature tubular furnace to undergo thermal annealing.

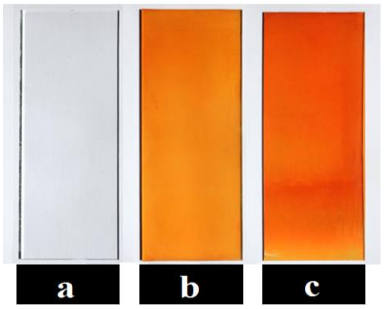

Fig. 1. Photographs of substrate free and elaborated samples a) substrate free b) as deposited for 3min c) deposited for 3min and annealed at 550°C for 2 hours.

2.2 Thin films characterization

The crystallographic structure of the α-Fe_2O_3 thin films in different dwelling time has been examined via an XPERT-PRO X-ray diffractometer system with a 30 kV, 30 mA, Cu Kα radiation with a wave length of 1.5406Å as operating conditions. Grain size was estimated via Xpert High Score. The band gap energy has been calculated through the optical transmittance spectrum using (UV–VIS spectrophotometer Shimadzu, Model 1800) operating in the wavelength 300-900nm range. The surface investigation was done with scanning electron microscope (SEM) using FEI Quanta 250 with a tungsten filament. Infrared analysis has been studied in the range 400-4000 cm^{-1} using Shimadzu IR-Infinity 1. All measurements were achieved at room temperature.

3. Results and discussion

3.1 Structural properties

The XRD patterns of as-deposited and annealed thin films are presented in Fig. 2. The observed peaks at 2θ: 24.23°, 33.24°,35.70°, 40.95°, 49.54°, 54.18°, 62.50°, and 64.17°correspond to lattice plane of (*012*), (*104*), (*110*), (*113*), (*024*), (*116*), (*214*) and (*300*), respectively. This result confirms that the elaborated films have a rhombohedral crystal structure and much well with the Joint Committee of Powder Diffraction System (as reported in reference (JCPDS No: 01.073-2234, with space group R-3c number 167). As shown in Fig.2, the orientation of the crystal is unsteady among dwelling time; before annealing, the films were multi-oriented with no preferred direction. Whereas after one hour of annealing the films are highly oriented along (*110*) plane, while after two hours they have two orientations along (*104*) and (*110*) planes, however after three hours,a preferred orientation along (*104*) was observed which point out growing in the crystallinity of the α-Fe_2O_3 thin films. At the limit of detection, no other components or phases appeared.

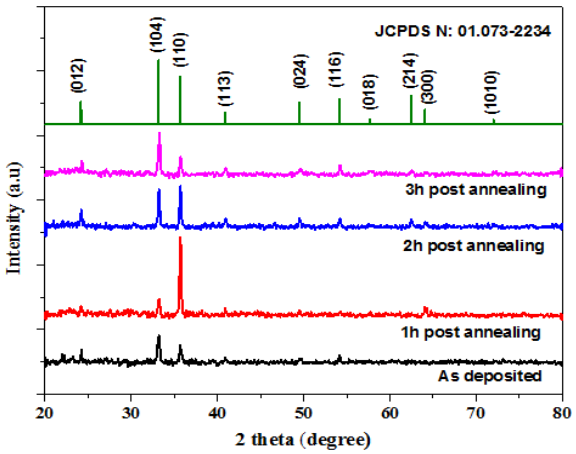

Fig. 2. X-ray diffraction patterns of sprayed hematite α-Fe_2O_3 thin films as function of heat annealing.

For more details, about the preferred growth directions, different texture coefficient *TC*(*hkl*) have been calculated from the X-ray data. *TC*(*hkl*) measures the relative degree of preferred orientation (PO) among crystal planes and is expressed via the following formula [34]:

$$TC(hkl) = \frac{I(hkl)/I_0(hkl)}{N^{-1}\sum_n^N I(hkl)/I_0(hkl)} \quad (1)$$

where *I(hkl)* is the measured relative intensity of a plane *(hkl)*, I_0*(hkl)* is the standard intensity of the plane *(hkl)* taken from the JCPDS data, *N* is the reflection number and *n* is the number of diffraction peaks. *TC*(*hkl*) values for (*012*), (*104*), (*110*) at different annealing time are illustrated in Fig. 3 it is evident that the films have different texture related to heating treatment duration; for one hour, the plane (*110*) have the highest *TC* value; after two hours of annealing, the planes (*104*), (*110*) have an approximate *TC* values which means that the films structure grown-up in the two directions with the same rate. The films annealed for three hours have a maximum *TC* value along (*104*) direction.

The lattice constants (*a* and *c*), for the rhombohedral phase structure, are determined by the relations [35]:

$$2d_{hkl}\sin(\theta) = n\lambda \quad (2)$$

and

$$\frac{1}{{d_{hkl}}^2} = \frac{4}{3a^2}(h^2 + k^2 + hk) + \frac{l^2}{c^2} \quad (3)$$

where 'd_{hkl}'and (*hkl*) are the inter-planer distance and Miller indices, respectively. The values of lattice parameters '*a*' and 'c' are listed in Table. 1. It is worth noting that the values which are close to the values of standard JCPDS data card, (a_0 =b_0 = 5.0325 Å and c_0 = 13.7404Å) are (a = b = 5.02896Å, c = 13.7255Å) of the samples annealed for 2 hours. Fig.4 shows the variation in the micro-strain, along the lattice constant ($\Delta a/a_0$ and $\Delta c/c_0$) of hematite α-Fe_2O_3 thin films for as-deposited and post annealed thin film over the bulk, is negative values which leads to suggest that the film grains are subbing an in-strain.

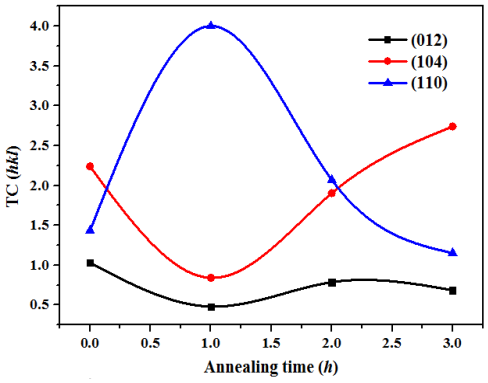

Fig. 3. Texture coefficient of hematite α-Fe_2O_3 thin films with different annealing times.

Table 1. Hematite parameters: d_{hkl} , Average grain size, Lattice Parameters of as-deposited and annealed samples.

Annealing Time (h)	*hkl*	*2θ* (°)	Lattice parameters (Å) $\Delta a=a-a_0$, $\Delta c=c-c_0$	Standard *d*(Å)	Calculated *d*(Å)	Average grain size (nm)
	012	24.240	a = 5.02854	3.68024	3.67178	
	104	33.239	b = 5.02854	2.69786	2.69545	
0h	110	35.705	c = 13.7272	2.51627	2.51472	40.84
	113	40.963	Δa = -0.0039	2.20537	2.20325	
	024	49.585	Δb = -0.0039	1.84012	1.83847	
	116	54.184	Δc = -0.0132	1.69366	1.69165	
	012	24.226	a = 5.02896	3.68024	3.67392	
	104	33.242	b = 5.02896	2.69786	2.69523	
1h	110	35.713	c = 13.7255	2.51627	2.51421	45.57
	113	40.904	Δa = -0.0035	2.20537	2.20632	
	024	49.512	Δb = -0.0035	1.84012	1.84103	
	116	54.213	Δc = -0.0148	1.69366	1.69197	
	012	24.240	a = 5.02896	3.68024	3.67329	
	104	33.230	b = 5.02896	2.69786	2.69537	
2h	110	35.709	c = 13.7259	2.51627	2.51448	48.54
	113	40.959	Δa = -0.0035	2.20537	2.20347	
	024	49.547	Δb = -0.0035	1.84012	1.83981	
	116	54.184	Δc = -0.0144	1.69366	1.69280	
	012	24.282	a = 5.0244	3.68024	3.66563	
	104	33.284	b = 5.0244	2.69786	2.69192	
3h	110	35.742	c = 13.7051	2.51627	2.51222	40.00
	113	40.976	Δa = -0.0080	2.20537	2.20262	
	024	49.613	Δb = -0.0080	1.84012	1.83751	
	116	54.229	Δc = -0.0353	1.69366	1.69151	

The crystalline sizes of thin films in different post annealing time given in Table1,were calculated for the more appeared peaks then make the average values by using Scherrer's formula [36].

$$D = \frac{0.9\,\lambda}{\beta cos\theta} \tag{4}$$

where D, β, λ, and θ are the crystallite size, the full width at half-maximum (FWHM) of the most intense diffraction peak, the X-ray wavelength (1.54056 Å) and Bragg angle, respectively. As can be shown in Table.1, the average D, increases monotonically with annealing time, from 40.84 nm for the as-deposited films to 48.54 nm for two hours annealing, then decreases to 40.00 nm for three hours annealing. Fig.5 gathers D variation with Urbach energy (Eu) for different annealing time. It is worth noting that D and Eu are oppositely varying revealing the theoretical results.

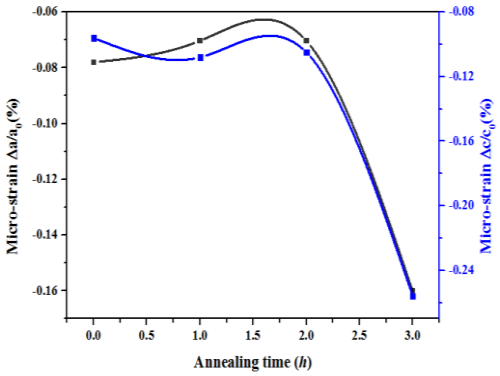

Fig. 4. Micro-strain of hematite α-Fe_2O_3 thin films upon annealing time.

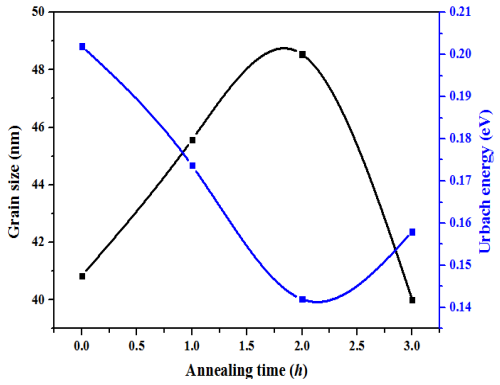

Fig. 5. Grain size and Urbach energy with various post annealing times.

3. 2 Surface morphology

The surface morphology of as-depositedand annealed iron oxide thin films (α-Fe_2O_3) are studied via SEM, Fig.6 shows the results with different annealing time: 0,1,2 and 3hours, respectively. The first common observation is that α-Fe_2O_3 films coat the substrate surface in smooth, uniform, and granular shape, the reason refers to the use of moving nozzle which riches the whole substrate surface isomorphically. The α-Fe_2O_3 thin films look to be more packed together with increasing time annealing. The as-deposited α-Fe_2O_3 thin films have nanoporous morphology with wheat-shaped grains (76.92 nm in size). For the annealed ones, As can be seen, the α-Fe_2O_3 thin films annealed for1 hour have egg-shaped grains and show nanoporous morphology (100 nm in size), while after two hours of annealing the grains have aspherical shape with nanoporous morphology also (142.85 nm in size). With increasing the annealing time to 3

hours, the films have mixture aspect with as deposited film and the annealed one for 1 hour but with smaller grain size (111.11 nm in size). Those observations and results are in good agreement with the XRD patterns.

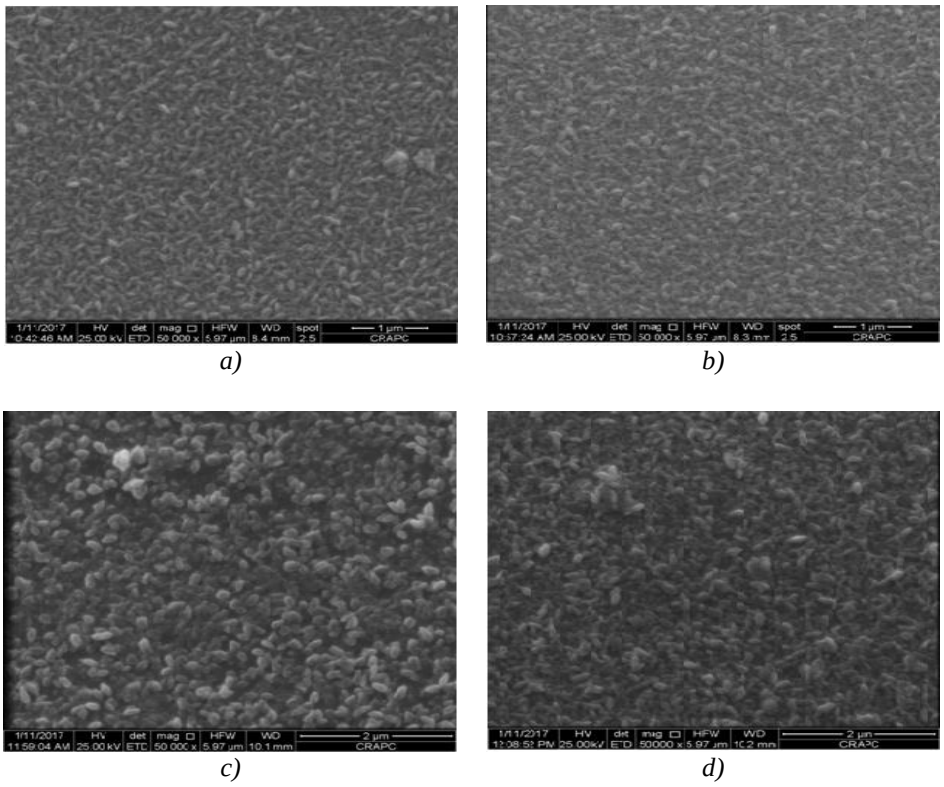

Fig. 6. Scanning electron microscopic image of hematite thin films: a) as deposited, (b), (c) and (d) annealed for 1, 2 and 3hours, respectively.

3. 3 Optical properties

Fig.7 shows the transmittance spectrum of hematite iron oxide thin films with different annealing time. As can be observed, the transmittance spectra of α-Fe_2O_3 thin films were found to be about 65% in the visible range, this value decreases with increasing annealing time, which refers to the fact that the crystalline structure of the films has to stack with thermal treatment. The low values of transmittance may be referred to light scattering from crystallographic imperfections. The films annealed for 2 and 3 hours have the same spectrum which means that they have the same optical behavior and leads to proclaiming that for optical properties there is no need to spend 3 hours for annealing. In order to investigate the band gap of the α-Fe_2O_3 thin films, Tauc'srelationis used [37]:

$$\alpha h\nu = A(h\nu - Eg)^n \tag{5}$$

where α, *h*, *v*, and E_g are the absorption parameter, Planck constant, the photon frequency and gap energy, respectively; ***A*** is a constant and *n* is taken 2 in based consideration that α-Fe_2O_3 has an indirect gap [38, 39]. The optical absorption data was used to generate plots of $(\alpha h\nu)^2$ vs $h\nu$, as shown in Fig. 8, leading to band gap energy of 2.135eV for the as-deposited film and 2.124, 2.116, and 2.111eV for the annealed films during 1, 2, and 3hours, respectively. Those values are in agreement with several previous works [40, 41].

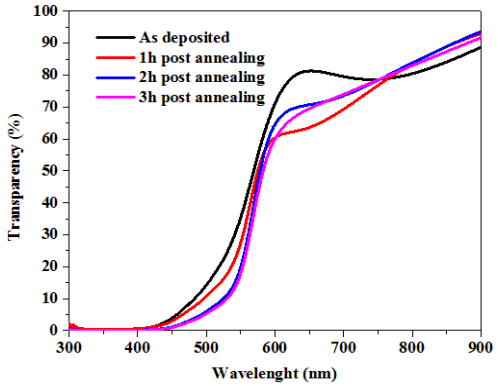

Fig. 7. Transparency spectrum of α-Fe_2O_3 thin films with 0-3hours post annealing at 550°C.

It is obvious that the annealed films for 2 and 3 hours have the same E_g value and they approximately have the same transmission spectra, which let us proclaim that there is no need to spend 3 hours for annealing. Optical values of the elaborated samples are given in Table 2.

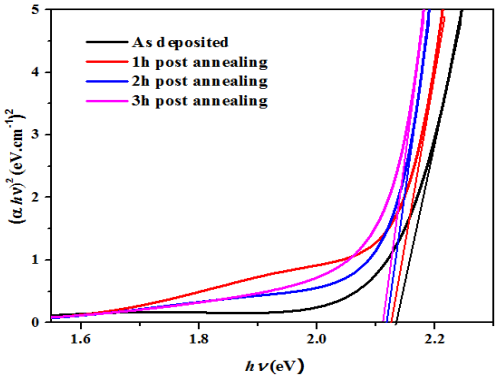

Fig. 8. Band gap (E_g) estimation from Tauc's relation for as sprayed α-Fe_2O_3 and annealed thin films.

Table 2. Optical gap, urbach energy, transmittance of as-deposited and annealed samples.

Annealing time	Optical gap E_g(eV)	Urbach energy E_u(meV)	Transmittance (%)
0h	2.135	202	71.56
1h	2.124	173	64.81
2h	2.116	142	60.91
3h	2.111	158	60.20

3. 4 FTIR

Fig. 9 shows the FTIR spectra of the α-Fe_2O_3 thin films with different annealing time. The spectra of all thin films exhibit two absorption bands which arecentered at approximately 470 and 543 cm^{-1}. The absorption peaks intensity and expansion increase directly with the post-annealing time. Those two bands are attributed to the Fe-O bond vibration of poly-crystalline hematite (α-Fe_2O_3) [42, 43]. Also, it is obvious that the curves differ from each other as reported by Rendon and Serna [42], where the authors proclaim that the IR spectrum of powdered hematite depends on particle shape. The peak at 922 cm^{-1} may be assigned to Fe-OH vibration modes[44], whereas the centered one at 1640 cm^{-1} indicates the presence of COO^- stretch mode[21, 45]. The absorption peaks observed at 2358 cm^{-1} is referred to the existence of CO_2 molecules which may refer to the

nearby atmosphere during samples preparation for IR mesurments [29]. The spectra exhibit the presence of OH peaks at (3455 cm^{-1}) [46] in our as-deposited samples and ones annealed for 1 and 3 hours only. No peak related to other groups was observed, which may be considered as an evidence of the purity of the prepared samples.

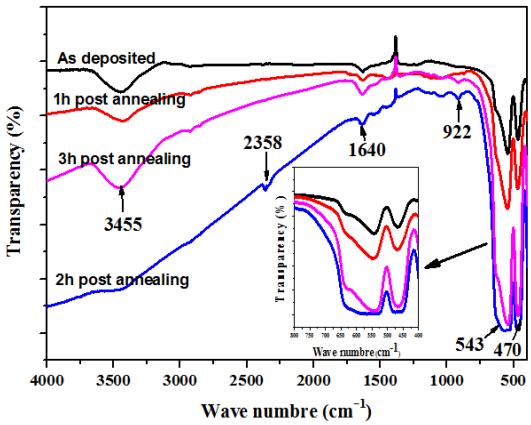

Fig. 9. FTIR spectrum of α-Fe_2O_3 thin films for (0-3 hours) post annealing at 550°C.

4. Conclusions

In this work, hematite iron oxide (α-Fe_2O_3) thin films were synthesized using spray pyrolysis with moving nozzle. The effect of post heat treatment at 550°C for periods: 0, 1, 2, 3 hours on their structural and optical properties have been studied. XRD analyses avowed the formation of hematite thin films structure along (*104*) and (*110*) as preferred orientations whereas the grain size varies upon time heat treatment and it was arranged in 40-48 nm. SEM images showed that all samples having smooth, granular and uniform morphology with variant shape upon post annealing time. The transparency of hematite thin films was averaged in 60-71% in the visible region, with an direct band gap in the range of 2.11-2.13eV. In α-Fe_2O_3 composition, FTIR spectrum affirms the abundance of Fe-O bond. All results insure that the best time of post-annealing was 2 hours.

Acknowledgments

This work was supported in part by El-Oued University for measuring UV-Visible data. X-ray diffraction data in this work were acquired with XPERT-PRO diffractometer which is supported by Physicochemical of mineral materials and its applications laboratory at Bordj cedria. We thank Ahmed Hichem Hamzaoui for his help and assistance to measure X-ray diffraction.

References

[1] W. Wu, Z. Wu, T. Yu, C. Jiang, W.-S. Kim, Science and technology of advanced materials, **16**(2), 023501 (2015).
[2] G. Zelmanov, R. Semiat, Water research **42**(1) 492 (2008).
[3] S. He, Y. Feng, J. Ni, Y. Sun, L. Xue, Y. Feng, Y. Yu, X. Lin, L. Yang, Chemosphere **147**, 195 (2016).
[4] S. He, Y. Feng, H. Ren, Y. Zhang, N. Gu, X. Lin, Journal of Soils and Sediments **11** (8), 1408 (2011).
[5] H. J. Shipley, K. E. Engates, A. M. Guettner, Journal of Nanoparticle Research **13** (6), 2387 (2011).

[6] Y. Cheng, X. Zhao, X. Liu, W. Sun, H. Ren, B. Gao, J. Wu, International Journal of Nanomedicine **10**, 727 (2015).
[7] C. Popa, A. Prodan, P. Chapon, C. Turculet, D. Predoi, Journal of Nanomaterials **5**, 2015 (2015).
[8] A. Ubale, M. Belkhedkar, Journal of Materials Science & Technology **31**(1), 1 (2015).
[9] D. K. Kim, M. Mikhaylova, Y. Zhang, M. Muhammed, Chemistry of Materials **15**(8), 1617 (2003).
[10] S. Schwarz, J. E. Wong, J. Bornemann, M. Hodenius, U. Himmelreich, W. Richtering, M. Hoehn, M. Zenke, T. Hieronymus, Nanomedicine: Nanotechnology, Biology and Medicine **8**(5), 682 (2012).
[11] A. Al-Hobaib, K. M. AL-Sheetan, L. El Mir, Materials Science in Semiconductor Processing **42**, 107 (2016).
[12] H. Parham, B. Zargar, M. Rezazadeh, Materials Science and Engineering: C, **32**(7), 2109 (2012).
[13] G. Zelmanov, R. Semiat, Separation and purification technology **80**(2), 330 (2011).
[14] M. Fondell, Acta Universitatis Upsaliensis, 2014.
[15] B. Issa, I. M. Obaidat, B. A. Albiss, Y. Haik, International journal of molecular sciences **14**(11), 21266 (2013).
[16] K. Woo, J. Hong, S. Choi, H.-W. Lee, J.-P. Ahn, C. S. Kim, S. W. Lee, Chemistry of Materials **16** (14), 2814 (2004).
[17] A. Ali, M. Z. Hira Zafar, I. ul Haq, A. R. Phull, J. S. Ali, A. Hussain, Nanotechnology, Science and Applications **9**, 49 (2016).
[18] D. Yokoyama, K. Namiki, H. Fukasawa, J. Miyazaki, K. Nomura, Y. Yamada, Journal of Radioanalytical and Nuclear Chemistry **272**(3), 631 (2007).
[19] A. M. Jubb, H. C. Allen, ACS Applied Materials & Interfaces **2**(10), 2804 (2010).
[20] S. Laurent, D. Forge, M. Port, A. Roch, C. Robic, L. Vander Elst, R. N. Muller, Chemical reviews **108**(6), 2064 (2008).
[21] R. Todorovska, S. Groudeva-Zotova, D. Todorovsky, Materials Letters **56**(5), 770 (2002).
[22] S. Kulkarni, C. Lokhande, Materials chemistry and physics **82**(1), 151 (2003).
[23] A. A. Akl, Applied Surface Science **221**(1), 319 (2004).
[24] J. Krysa, M. Zlamal, S. Kment, M. Brunclikova, Z. Hubicka, Molecules **20**(1), 1046 (2015).
[25] R. Schrebler, K. Bello, F. Vera, P. Cury, E. Muñoz, R. del Río, H. G. Meier, R. Córdova, E. A. Dalchiele, Electrochemical and solid-state letters **9**(7), C110 (2006).
[26] R. V. Kumar, Y. Diamant, A. Gedanken, Chemistry of Materials **12**(8), 2301 (2000).
[27] G. Binitha, M. Soumya, A. A. Madhavan, P. Praveen, A. Balakrishnan, K. Subramanian, M. Reddy, S. V. Nair, A. S. Nair, N. Sivakumar, Journal of Materials Chemistry A **1**(38), 11698 (2013).
[28] T. Mariño-Otero, M. Oliver-Tolentino, M. A. Aguilar-Frutis, G. Contreras-Martínez, E. Pérez-Cappe, E. Reguera, international journal of hydrogen energy **40**(17), 5831 (2015).
[29] B. K. Ozcelik, C. Ergun, Ceramics International **41**(2), 1994 (2015).
[30] S. Shinde, R. Bansode, C. Bhosale, K. Rajpure, Journal of Semiconductors **32**(1), 013001 (2011).
[31] A. A. Yadav, T. Deshmukh, R. Deshmukh, D. Patil, U. Chavan, Thin Solid Films **616,** 351 (2016).
[32] K. B. Narayanan, N. Sakthivel, Advances in colloid and interface science **156**(1), 1 (2010).
[33] M. Shah, D. Fawcett, S. Sharma, S. K. Tripathy, G. E. J. Poinern, Materials **8**(11), 7278 (2015).
[34] P. Paufler, C. S. Barrett, T. B. Massalski, Crystal Research and Technology **16**(9), 982 (1981).
[35] L. Dghoughi, B. Elidrissi, C. Bernede, M. Addou, M. A. Lamrani, M. Regragui, H. Erguig, Applied Surface Science **253** (4), 1823 (2006).
[36] P. Scherrer, Göttinger Nachrichten Math. Phys. **2,** 98 (1918).
[37] J. Tauc, R. Grigorovici, A. Vancu, physica status solidi (b), **15**(2), 627 (1966).
[38] J. Desai, H. Pathan, S.-K. Min, K.-D. Jung, O.-S. Joo, Applied surface science **252**(6), 2251 (2006).

[39] R. N. Goyal, D. Kaur, A. K. Pandey, Materials Chemistry and Physics **116**(2), 638 (2009).
[40] B. Ouertani, J. Ouerfelli, M. Saadoun, H. Ezzaouia, B. Bessaïs, Thin Solid Films **516**(23), 8584 (2008).
[41] O. Akhavan, Applied Surface Science **257**(5), 1724 (2010).
[42] J. L. Rendon, C.J. Serna, Clay Miner **16**(4), 375 (1981).
[43] J. Desai, H. Pathan, S.-K. Min, K.-D. Jung, O. S. Joo, Applied surface science **252**(5), 1870 (2005).
[44] M. Belkhedkar, A. Ubale, International Journal of Materials and Chemistry **4** (5), 109 (2014).
[45] C. Zhang, Z. Yu, G. Zeng, B. Huang, H. Dong, J. Huang, Z. Yang, J. Wei, L. Hu, Q. Zhang, Chemical Engineering Journal **284**, 247 (2016).
[46] J. Ding, Q. Zhong, S. Zhang, Journal of Molecular Catalysis A: Chemical **393**, 222 (2014).